scientific reports

Check for updates

OPEN

Theoretical studies on the two-photon absorption of II–VI semiconductor nano clusters

Deyang Yu[1,3], YangYang Hu[1,2], Guiling Zhang[1,2]✉, Weiqi Li[3,4,5]✉ & Yongyuan Jiang[3,4]✉

Semiconductor clusters, Zn_nO_n, Zn_nS_n, and Cd_nS_n (n = 2–8), were optimized and the corresponding stable structures were acquired. The symmetry, bond length, bond angle, and energy gap between HOMO and LUMO were analyzed. According to reasonable calculation and comparative analysis for small clusters Zn_2O_2, Zn_2S_2, and Cd_2S_2, an effective method based on density function theory (DFT) and basis set which lay the foundation for the calculation of the large clusters have been obtained. The two-photon absorption (TPA) results show that for the nano clusters with planar configuration, sizes play important role on the TPA cross section, while symmetries determine the TPA cross section under circumstance of 3D stable structures. All our conclusions provide theoretical support for the development of related experiments.

Due to the three-dimensional (3D) quantum confinement effect, II–VI semiconductor clusters are proved to have significant nonlinear optical (NLO) properties and are widely used in physics, chemistry, and biomedical engineering[1,2]. Compared with bulk materials, nano clusters have greater two-photon absorption (TPA) cross section and nonlinear refractivity, and the absorption peak and absorption coefficient are closely related with their sizes, structures, specific surface area, surface defect, ligand type, way of bonding and so forth[3–8]. So far, it is possible to synthesize II–VI group semiconductor quantum dots using collochemistry method, and the researches of NLO properties mostly focuses on the second/third order susceptibility. Amit D. Lad et al. used the open-hole Z-scanning technique to investigate the third order NLO properties of ZnSe with different sizes[9]. It shows that the absorption cross section increased with decreased diameter of quantum dots. Xiaobo Feng and Wei Ji investigated the TPA of nano semiconductor crystal with different shapes and sizes[10]. They compared the absorption cross section of CdS nano sphere (4.45 nm in diameter) and CdS nano cylinder (4.4 nm in diameter and 43 nm in length). It turns out that CdS nano sphere had an absorption cross section of 10^3 GM and $10^4 \sim 10^5$ GM for CdS nano cylinder, which can be explained that the reduced symmetry of nano cylinder resulted in the division of energy state, and this leads to an increased density of energy state.

Although the great improvements in the synthesis of the semiconductor nano clusters[11–14], it is still difficult to obtain samples with uniform sizes and controllable shapes experimentally, further realize the measurement of optical properties of nano clusters with the same size and morphology. Fortunately, theoretical calculations can fill the gap in this regard, such as the prediction for experiments, and the analysis and study of the experimental results. Up to now, the investigation of mechanism and computation method of semiconductor nano clusters' spectra has made some achievable breakthrough[15–18]. There are studies about relatively stable semiconductor quantum dots and their electronic properties using first-principles theory, and it has been explained how the stability of system is determined by the width of energy gap between conduction band and valence band, as well as how the energy gap is determined by the system's bonding energy. Perry et al. utilized experiments combined with theoretical calculations to systematically compare the one-photon and two-photon spectroscopy of CdSe nano clusters and organic molecules[19]. The results pointed out that semiconductor clusters over 3 nm had NLO properties with bulk materials and could be described using effective mass model.

[1]School of Materials Science and Chemical Engineering, Harbin University of Science and Technology, Harbin 150080, China. [2]Key Laboratory of Green Chemical Technology of College of Heilongjiang Province, Harbin University of Science and Technology, Harbin 150080, China. [3]School of Physics, Harbin Institute of Technology, Harbin 150001, China. [4]Key Lab of Micro-Optics and Photonic Technology of Heilongjiang Province, Harbin 150001, China. [5]State Key Laboratory of Intense Pulsed Radiation Simulation and Effect, Xi'an 710024, China. ✉email: guiling-002@163.com; tccliweiqi@hit.edu.cn; jiangyy@hit.edu.cn

Despite the reported TPA from experiments and theories, there is still rare researches on the structural information and evolution rules of semiconductor nano clusters, and the existing studies still have much stochasticity. The lack of understanding the relevancy of the cluster structures on its properties makes it necessary to establish a comprehensive theoretical analysis. Aimed at exploring the correlation between the TPA of small nano clusters (Zn_nO_n, Zn_nS_n, and Cd_nS_n, n = 2–8) and their structures, the present paper are organized as follows: (1) the choice of the appropriate density functional method and basis set for predicting the NLO response of the semiconductor nano clusters; (2) the rules of changing TPA cross section with structures. This will be of great importance to the research of the semiconductor nano clusters, because on one hand, an effective method and basis set for the calculation of the structures of large clusters will be obtained. And on the other hand, the effects of cluster sizes and structure on the TPA will be studied, the rules will be summarized and explained. They all provide theoretical support for the development of related experiments.

Computational method

In order to find out the most suitable methods based on density functional theory (DFT) for calculating the TPA cross section of the semiconductor nano clusters, eight different methods were chosen for the exploration, including local density approximation functional SVWN[20–23]; generalized gradient approximation BPW91[24–29]; hybrid functional B3LYP, DBLYP, X3LYP, and BHandLYP[30–33]; long range correct functional CAM-B3LYP[34]; double hybrid functional B2PLYP[35]. By using the above methods, the first four transition energies of Zn_2O_2 and Zn_2S_2 were calculated and compared with that obtained from the high-precision coupled cluster method including singles and doubles fully (CCSD)[36–39], and a proper DFT method was chosen. The all-electronic basis set 6-31G* was used for the calculation of Zn with small atomic numbers. Due to the large atomic number of Cd, the all-electron basis set is not applicable, so the pseudopotential basis set is considered. The transition energies for the first six excited states of Cd_2S_2 were calculated using three different pseudopotential basis sets cc-pVDZ-pp, LANL2DZ, and SDD as well as the aug-cc-pVDZ-pp basis set, and the suitable pseudopotential basis sets to be used in the calculation of larger systems was selected.

Different structures of II–VI group semiconductor nano clusters of Zn_nO_n, Zn_nS_n, and Cd_nS_n, n = 2–8 were generated, and the nano clusters which contained 4 to 16 atoms were optimized by Gaussian09 software[40]. The TPA cross-section (δ_{TPA}) were evaluated by means of calculating the two-photon transition moment matrix elements ($S_{\alpha\beta}$) in the Dalton package[41–45]. For two-photon absorption, the $S_{\alpha\beta}$ expressed as

$$S_{\alpha\beta} = \sum_n \left[\frac{\langle 0|\mu_\alpha|n\rangle\langle n|\mu_\beta|f\rangle}{\omega_n - \frac{\omega_f}{2}} + \frac{\langle 0|\mu_\beta|n\rangle\langle n|\mu_\alpha|f\rangle}{\omega_n - \frac{\omega_f}{2}} \right] \tag{1}$$

For the absorption of two photons of identical energy, where n ranges from the ground state 0 to the final excited state f. The calculated $S_{\alpha\beta}$ can then be used to obtain the δ_{TPA}, as shown in Eq. (2)

$$\delta_{TPA} = \frac{1}{30} \sum_{\alpha\beta} FS_{\alpha\alpha}S_{\beta\beta} + GS_{\alpha\beta}S_{\alpha\beta} + HS_{\alpha\beta}S_{\beta\alpha} \tag{2}$$

where the summations are performed over the molecular axes (i.e., x, y, and z in Cartesian coordinates), and F, G, and H depend on the polarization vectors of the incoming photons. Assuming that the incident radiation is linearly polarized monochromatic light, the transition moment for TPA (in atomic units) is

$$\delta_{TPA} = \frac{1}{30} \sum_{\alpha,\beta} 2S_{\alpha\alpha}S^*_{\beta\beta} + 4S_{\alpha\beta}S^*_{\beta\beta} \tag{3}$$

In view of the relation to the experimental measurements, the δ_{TPA} is usually expressed in terms of Göppert-Mayer (GM) units, where 1 GM is 10^{-50} cm^4 s photon^{-1} molecule^{-1}. As a result, the relationship between the macroscopic TPA cross section in GM (σ_{TPA}) and the immediate computation output in atomic units (δ_{TPA}) is given by

$$\sigma_{TPA} = \frac{4\pi^2 a_0^5 \alpha}{15c} \frac{\omega_f^2}{\Gamma} \delta_{TPA} \tag{4}$$

where α is the fine structure constant, a_0 is the Bohr radius, c is the speed of light, ω_f is the excitation energy for the $0 \rightarrow f$ transition, and Γ is the broadening width.

Results and discussion

Errors of the first four excited state transition energies between CCSD and the eight DFT methods for Zn_2O_2 are shown in Table 1 and Fig. 1. It can be clearly seen from Table 1 that the errors for the transition energies of the first four excited states of Zn_2O_2 between CAM-B3LYP and CCSD are − 0.09, − 0.09, − 0.09, and − 0.03, much smaller than the other seven DFT methods. The largest error comes from BHandLYP with − 2.58, − 2.43, − 1.77, and − 1.67, respectively. According to the above results analysis, the accuracy of the eight DFT methods sort from the largest to the smallest are: CAM-B3LYP > X3LYP > B3LYP > DBLYP > BPW91 > SVWN > B2LYP > BHandLYP.

Errors of the first four excited state transition energies between CCSD and the eight DFT methods for Zn_2S_2 are shown in Table 2 and Fig. 2. It can be seen from the data that errors for the transition energies of the first four excited states of Zn_2S_2 between CAM-B3LYP and CCSD are also the smallest (0.06, − 0.05, 0.04, and 0.13, respectively). The maximal errors appear in SVWN with the values 0.65, 0.50, 0.81, and 0.77, respectively. The accuracy of the eight DFT methods sort from largest to smallest are:

Methods\excited state	$S_0 \rightarrow S_1$	$S_0 \rightarrow S_2$	$S_0 \rightarrow S_3$	$S_0 \rightarrow S_4$
SVWN	− 0.59	− 0.43	− 0.69	− 0.48
BPW91	0.49	0.55	0.65	0.45
B3LYP	0.23	0.18	0.31	0.34
BHandHLYP	− 2.58	− 2.43	− 1.77	− 1.67
DBLYP	0.53	0.40	0.69	− 0.50
X3LYP	0.21	0.16	0.28	0.33
CAMB3LYP	− 0.09	− 0.09	− 0.09	− 0.03
B2PLYP	0.90	1.42	0.61	0.53

Table 1. Errors for the transition energies of the first four excited states between CCSD and the eight different DFT methods for Zn_2O_2.

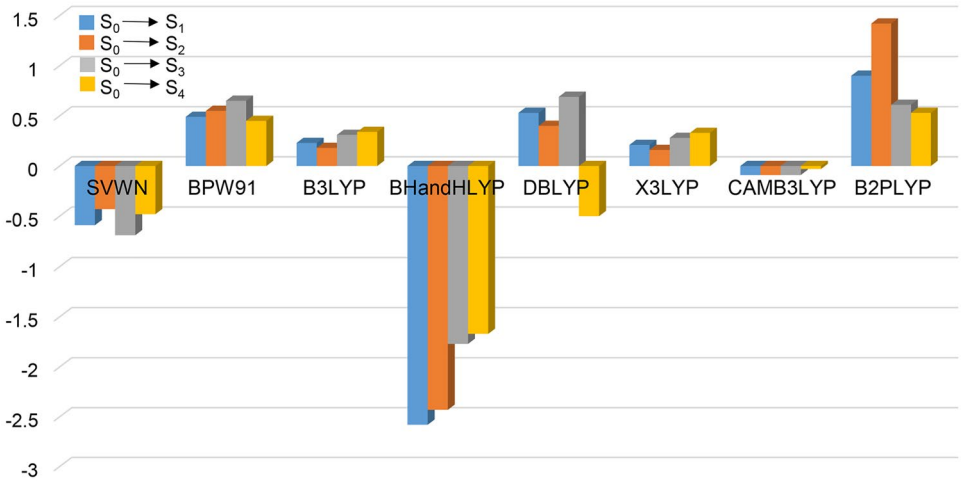

Figure 1. Errors for the transition energies of the first four excited states between CCSD and the eight different DFT methods for Zn_2O_2.

Methods\excited state	$S_0 \rightarrow S_1$	$S_0 \rightarrow S_2$	$S_0 \rightarrow S_3$	$S_0 \rightarrow S_4$
SVWN	0.65	0.50	0.81	0.77
BPW91	0.50	0.40	0.70	0.67
B3LYP	0.34	0.27	0.50	0.52
BHandHLYP	− 0.25	− 0.26	− 0.1	− 0.00
DBLYP	0.52	0.42	0.75	0.70
X3LYP	0.33	0.26	0.48	0.51
CAMB3LYP	0.06	− 0.05	0.04	0.13
B2PLYP	− 0.30	− 0.29	− 0.15	− 0.05

Table 2. Errors for the transition energies of the first four excited states between CCSD and the eight different DFT methods for Zn_2S_2.

CAM-B3LYP > BHandLYP > B2LYP > X3LYP > B3LYP > BPW91 > DBLYP > SVWN. In summary, CAM-B3LYP is more suitable for the calculating of the TPA for the II–VI semiconductor clusters, and it will be selected to predict the σ_{TPA} value of Zn_nO_n, Zn_nS_n, and Cd_nS_n, n = 2–8 in present work.

The errors of the first six excited state transition energies for Cd_2S_2 between cc-pVDZ-pp, LANL2DZ, SDD and the more precise aug-cc-pVDZ-pp basis sets are as follows: SDD > LANL2DZ > cc-pVDZ-pp, as shown in Fig. 3. The error of SDD is the largest, and those of cc-pVDZ-pp and LANL2DZ are not much different. Although the error of cc-pVDZ-pp is a little smaller than that of LANL2DZ, considering the higher calculation efficiency of LANL2DZ than that of cc-PVDZ-pp, the LANL2DZ is chosen in the calculation of Cd clusters. According to the above analysis, the σ_{TPA} value of the II–VI group semiconductors nano clusters were quantified by CAM-B3LYP. The Zn atoms used 6-31G*, and LANL2DZ was used for the Cd atoms.

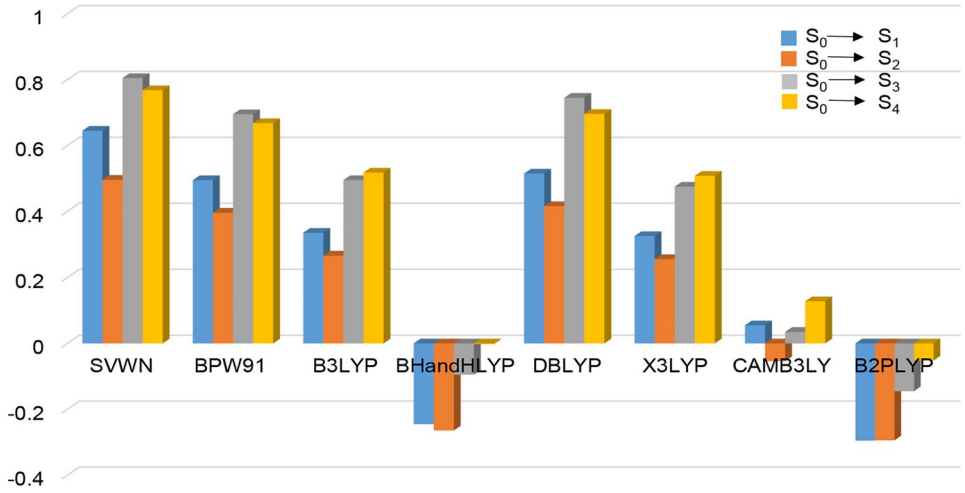

Figure 2. Errors for the transition energies of the first four excited states between CCSD and the eight different DFT methods for Zn_2S_2.

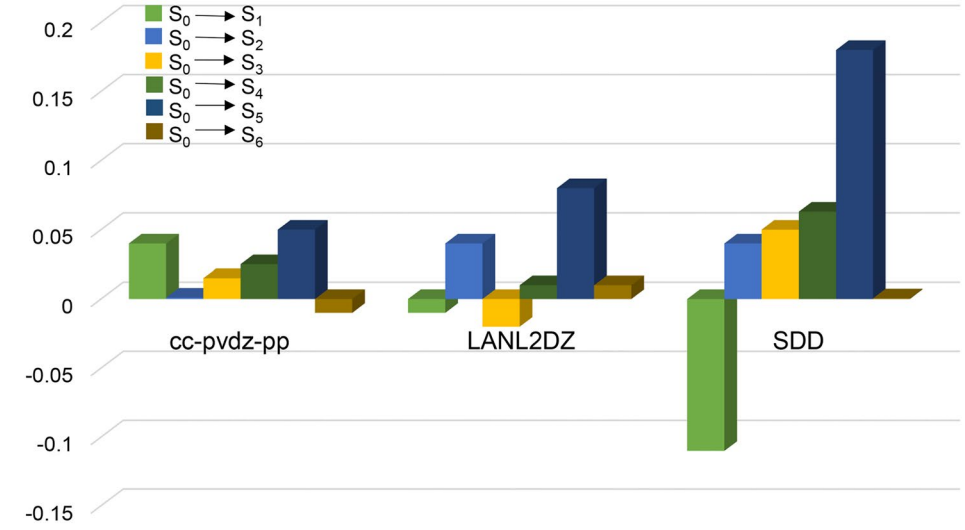

Figure 3. Errors of the first six excited state transition energies between aug-cc-pVDZ-pp and other three basis sets for Cd_2S_2.

The possible stable isomers of nano clusters with different size have been researched in the potential energy surface (PES). For NLO calculation, only isomers with lowest energy as shown in Fig. 4 have been considered. Table 3 gives the symmetry, bond length, bond angle, and energy gap between HOMO and LUMO of Zn_nO_n, Zn_nS_n, and Cd_nS_n, n = 2–8 at their lowest energy structures. In present work, the stable configurations on PES are consistent with previous study[46]. For Zn_nO_n (n = 2–8) with smaller atomic numbers, the framework changes from two-dimensional (2D) to 3D when n = 8. With regard to the 2D framework, the bond length of Zn–O ranges from 1.77 Å to 1.89 Å, the bond angle of –O–Zn–O– ranges of ranges from102.70° to 179.38°, and ranges from77.30° to 126.10° for –Zn–O–Zn–. In addition, the bond length tends to decrease, while the bond angle tends to increase with increasing the number of n due to relaxation of ring tension. The range of HOMO–LUMO energy gap is 4.37 to 4.72 eV. The value of the HOMO–LUMO energy gap is larger in 2D structures than that in 3D structure. The unusual HOMO–LUMO energy gap comes from Zn_2O_2 with the value 2.70 eV, suggesting that it may appear properties distinguished from the other 2D structures.

In the case of Zn_nS_n (n = 2–8), maintaining the elements of IIB group but augmenting the atomic number of the VIA element, the bond length, bond angle, and energy gap between HOMO and LUMO have different characters from those in Zn_nO_n (n = 2–8). Due to the larger atomic radius of S, the stable clusters change from 2 to 3D when n = 6. As increasing the atomic number of the IIB elements further, the stable clusters begin to stay in the form of 3D frameworks when n = 5 in Cd_nS_n (n = 2–8). To sum up, the larger the radius of atoms, the more stable of the clusters in their 3D forms. The HOMO–LUMO energy gaps of Zn_nO_n, Zn_nS_n, and Cd_nS_n,

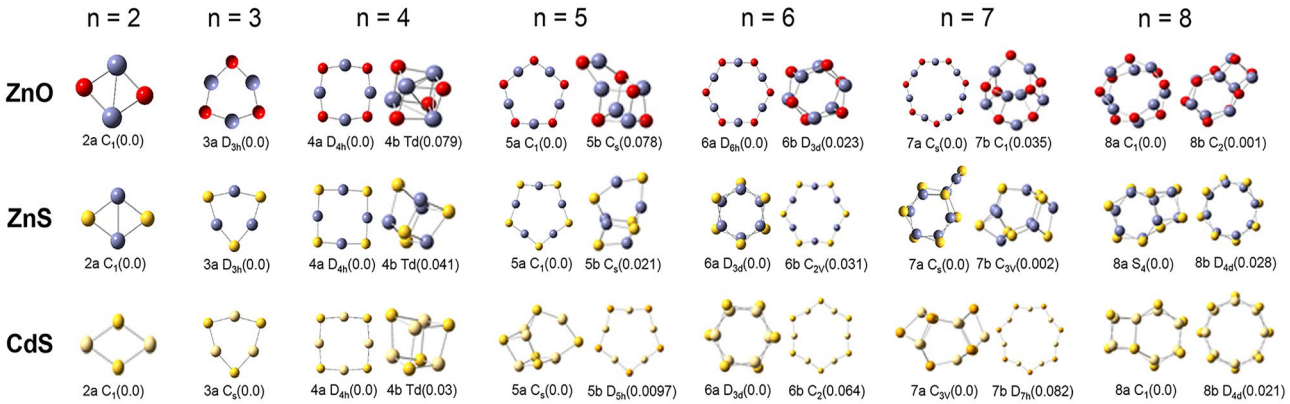

Figure 4. Optimized structures of Zn_nO_n, Zn_nS_n, and Cd_nS_n, n = 2–8 at the lowest/lower energy states. The energy from low to high is labeled by a and b. The values in the brackets are the energy difference to the lowest energy state of the corresponding structure.

n	Symmetry	Zn–O (Å)	–O–Zn–O– (°)	–Zn–O-Zn– (°)	E_g (eV)
2	C_1	1.89	102.70	77.30	2.70
3	D_{3h}	1.83	145.10	94.90	4.37
4	D_{4h}	1.80	164.66	105.34	4.60
5	C_1	1.79	174.17	113.91	4.72
6	D_{6h}	1.78	179.38	120.62	4.59
7	C_s	1.77	177.58	126.10	4.68
8	C_1	1.87 to 2.15	92.95 to 151.28	84.99 to 118.61	4.01
		Zn–S(Å)	**–S–Zn–S– (°)**	**–Zn–S–Zn– (°)**	**E_g (eV)**
2	C_1	2.27	113.87	66.13	2.77
3	D_{3h}	2.21	157.16	82.84	4.17
4	D_{4h}	2.18	176.63	93.44	4.46
5	C_1	2.18	173.34	101.34	4.46
6	D_{3d}	2.31 to 2.47	101.67 to 140.13	73.92 to 95.46	3.87
7	C_s	2.15 to 2.46	100.15 to 139.90	73.38 to 109.50	3.49
8	S_4	2.29 to 2.43	100.36 to 137.03	72.98 to 104.63	4.05
		Cd–S(Å)	**–S–Cd–S– (°)**	**–Cd–S–Cd– (°)**	**E_g (eV)**
2	C_1	2.71	55.29	124.72	1.81
3	C_s	2.48	152.77	87.29	3.33
4	D_{4h}	2.46	172.61	97.39	3.45
5	C_s	2.55	102.01 to 126.65	76.83 to 94.88	2.63
6	D_{3d}	2.59 to 2.75	98.65 to 137.79	78.21 to 100.23	3.18
7	C_{3V}	2.65	110.41 to 125.25	78.89 to 104.61	2.96
8	C_1	2.60	49.54 to 134.17	79.40 to 108.42	3.18

Table 3. The symmetry, bond length, bond angle, and energy gap between HOMO and LUMO (E_g) of Zn_nO_n, Zn_nS_n, and Cd_nS_n, n = 2–8 at their lowest energy structures.

n = 2–8 in their 2D forms are larger than those in their 3D forms, except n = 2. For smallest cluster (n = 2), due to the delocalization of electrons in the whole molecule, the molecular energy gap becomes particularly small.

The calculated TPA cross sections of Zn_nO_n, Zn_nS_n and Cd_nS_n, n = 2–8 are shown in Table 4 and Fig. 5. For the planar clusters of Zn_nO_n, the largest value of σ_{TPA} comes from Zn_2O_2 with the value 15.37 GM at 552.30 nm. The TPA cross section decreases with n increasing from 2 to 6, and the value drops to 2.14 GM when n = 6. However, the value of σ_{TPA} is enhanced to 8.15 GM at n = 7, the junction between the 2D and 3D structure. For Zn_nS_n clusters of different sizes, their two-photon absorption cross sections vary from 2.47 to 9.50 GM. According to simple model as following in Eq. (5)[47], the two-photon absorption cross section is inversely proportional to the square of the transition energy of first excited state and directly proportional to the transition matrix element. As shown in Table S1, all Zn_nS_n clusters have similar first excitation energy, thus their two-photon absorption cross sections do not differ much.

Zn_nO_n	2	3	4	5	6	7	8
σ_{TPA}	15.37	11.32	9.57	4.39	2.14	8.15	0.57
λ_{max}	552.30	414.72	434.33	372.37	393.65	379.20	576.74
Zn_nS_n	2	3	4	5	6	7	8
σ_{TPA}	4.50	5.46	5.92	3.76	5.87	9.50	2.47
λ_{max}	601.90	399.36	481.55	467.04	514.52	475.10	492.06
Cd_nS_n	2	3	4	5	6	7	8
σ_{TPA}	189.57	10.47	0.33	0.75	0.25	3.79	15.85
λ_{max}	536.80	510.29	515.59	596.15	670.27	712.64	589.07

Table 4. The TPA cross section σ_{TPA} (GM) and their corresponding maximum absorption wavelength λ_{max} (nm) of Zn_nO_n, Zn_nS_n, and Cd_nS_n, n = 2–8.

$$\delta_{TPA} \propto \frac{M_{01}^2 M_{1n}^2}{(E_{01}^2 - E_{1n})} \tag{5}$$

Combined with the HOMO–LUMO energy gap mentioned above, Zn_nO_n, Zn_nS_n and Cd_nS_n nano clusters present excellent two-photon absorption properties due to planar and compact configuration leading to good delocalization of electrons. Especially, for Cd_2S_2, because cadmium and sulfur atoms have a larger radius and smaller electronegativity, valence electrons are more easily polarized thus it has a very large NLO response. Different from the 2D cases, the TPA cross sections of both Zn_nS_n and Cd_nS_n with 3D geometry show no obvious correlation with the number of n. The largest value of σ_{TPA} for Zn_nS_n in the 3D case is 9.50 GM at 475.10 nm, from Zn_7S_7. On the other hand, the largest σ_{TPA} value for Cd_nS_n is 15.85 GM at 589.07 nm, from Cd_8S_8.

By referring the symmetry of the 3D structures, the symmetry of Zn_7S_7 and Cd_8S_8 is C_s and C_1, respectively, lower than the other corresponding 3D clusters. In other words, the symmetry has significant influence on the TPA of the 3D nano clusters, the lower the symmetry the higher the TPA cross section.

Conclusions

Semiconductor clusters of Zn_nO_n, Zn_nS_n, and Cd_nS_n (n = 2–8) were optimized and the corresponding stable structures were acquired. The symmetry, bond length, bond angle, and energy gap between HOMO and LUMO were analyzed. The results show that the larger the radius of atoms, the more stable of the clusters in their 3D forms. According to reasonable calculation and comparative analysis for Zn_2O_2, Zn_2S_2, and Cd_2S_2, CAM-B3LYP is more suitable for the calculating of the TPA cross sections for the II–VI semiconductor nano clusters, and LANL2DZ for the Cd atoms.

For the 2D nano clusters, sizes play important role on the TPA cross section. Generally, the value of TPA cross section will become abnormal at the junction between the 2D and 3D structures. In the case of the 3D nano clusters, the value TPA cross section are determined by the symmetries, the lower the symmetry the higher the TPA cross section.

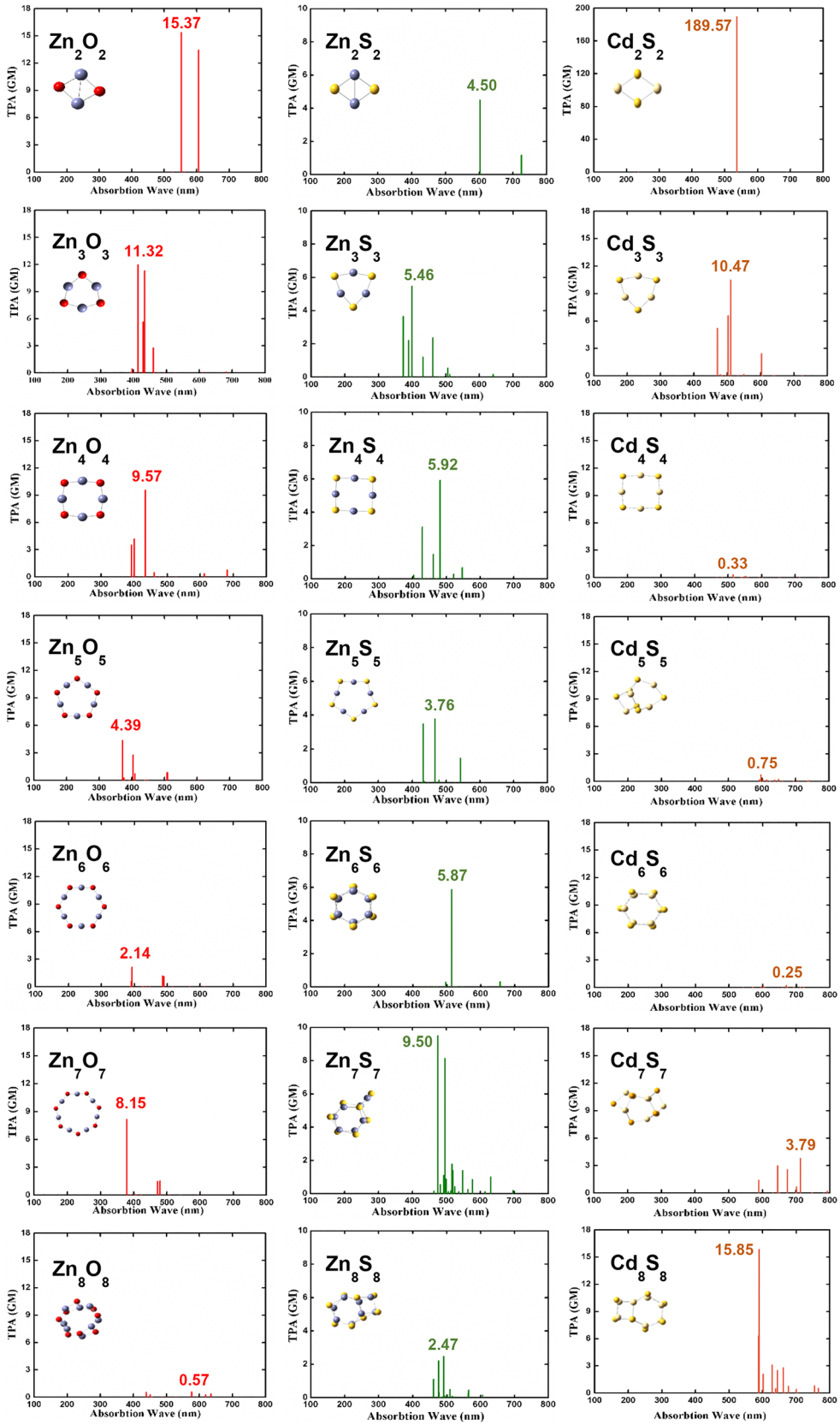

Figure 5. Calculated TPA cross sections of Zn_nO_n, Zn_nS_n, and Cd_nS_n, n = 2–8.

Received: 30 August 2021; Accepted: 17 December 2021
Published online: 07 January 2022

References

1. Irimpan, L. Spectral and nonlinear optical characterization of ZnO nanocomposites. *Sci. Adv. Mater.* https://doi.org/10.1166/sam.2010.1083 (2019).
2. Rana, M. & Chowdhury, P. Studies on size dependent structures and optical properties of CdSeS clusters. *J. Clust. Sci.* **31**(5), 1111–1121 (2020).
3. Nyk, M., Wawrzynczyk, D., Szeremeta, J. & Samoc, M. Spectrally resolved size-dependent third-order nonlinear optical properties of colloidal CdSe quantum dots. *Appl. Phys. Lett.* **100**(4), 041102 (2012).
4. Pan, L., Tamai, N., Kamada, K. & Deki, S. Nonlinear optical properties of thiol-capped CdTe quantum dots in nonresonant region. *Appl. Phys. Lett.* **91**(5), 051902 (2007).
5. Zhou, Z. *et al.* Surface states controlled broadband enhancement of two-photon absorption. *Appl. Phys. Lett.* **103**(23), 231111 (2013).
6. Chen, J. *et al.* Size-and wavelength-dependent two-photon absorption cross-section of CsPbBr 3 perovskite quantum dots. *J. Phys. Chem. Lett.* **8**(10), 2316–2321 (2017).
7. Nguyen, K. A., Pachter, R. & Day, P. N. Calculations of one-and two-photon absorption spectra for molecular metal chalcogenide clusters with electron-acceptor ligands. *J. Phys. Chem. A* **121**(8), 1748–1759 (2017).
8. Khan, Z. R. *et al.* Structural, linear and third order nonlinear optical properties of sol-gel grown Ag-CdS nanocrystalline thin films. *J. Electron. Mater.* **48**(2), 1122–1132 (2019).
9. Lad, A. D., Kiran, P. P., More, D., Kumar, G. R. & Mahamuni, S. Two-photon absorption in ZnSe and Zn Se/Zn S core/shell quantum structures. *Appl. Phys. Lett.* **92**(4), 043126 (2008).
10. Feng, X. & Ji, W. Shape-dependent two-photon absorption in semiconductor nanocrystals. *Opt. Express* **17**(15), 13140–13150 (2009).
11. Yang, J. *et al.* Chemical synthesis, doping, and transformation of magic-sized semiconductor alloy nanoclusters. *J. Am. Chem. Soc.* **139**(19), 6761–6770 (2017).
12. Salavati-Niasari, M., Davar, F. & Mazaheri, M. Synthesis and characterization of ZnS nanoclusters via hydrothermal processing from [bis (salicylidene) zinc (II)]. *J. Alloy. Compd.* **470**(1–2), 502–506 (2009).
13. Xia, Y.-S. & Zhu, C.-Q. Aqueous synthesis of luminescent magic sized CdSe nanoclusters. *Mater. Lett.* **62**(14), 2103–2105 (2008).
14. Liu, B. *et al.* Photoluminescence and structural characteristics of CdS nanoclusters synthesized by hydrothermal microemulsion. *J. Appl. Phys.* **89**(2), 1059–1063 (2001).
15. Botti, S. & Marques, M. A. Identification of fullerene-like CdSe nanoparticles from optical spectroscopy calculations. *Phys. Rev. B* **75**(3), 035311 (2007).
16. Elward, J. M., Irudayanathan, F. J., Nangia, S. & Chakraborty, A. Optical signature of formation of protein corona in the firefly luciferase-CdSe quantum dot complex. *J. Chem. Theory Comput.* **10**(12), 5224–5228 (2014).
17. Nguyen, K. A., Day, P. N. & Pachter, R. Understanding structural and optical properties of nanoscale CdSe magic-size quantum dots: Insight from computational prediction. *J. Phys. Chem. C* **114**(39), 16197–16209 (2010).
18. Nguyen, K. A., Pachter, R. & Day, P. N. Computational prediction of structures and optical excitations for nanoscale ultrasmall ZnS and CdSe clusters. *J. Chem. Theory Comput.* **9**(8), 3581–3596 (2013).
19. Makarov, N. S. *et al.* Two-photon absorption in CdSe colloidal quantum dots compared to organic molecules. *ACS Nano* **8**(12), 12572–12586 (2014).
20. Hohenberg, P. & Kohn, W. Inhomogeneous electron gas. *Phys. Rev.* **136**(3B), B864–B871. https://doi.org/10.1103/PhysRev.136.B864 (1964).
21. Kohn, W. & Sham, L. J. Self-consistent equations including exchange and correlation effects. *Phys. Rev.* **140**(4A), A1133 (1965).
22. Slater, J. C. Quantum theory of molecular and solids. The self-consistent field for molecular and solids. *Phys. Today* **27**, 49–50 (1974).
23. Vosko, S. H., Wilk, L. & Nusair, M. Accurate spin-dependent electron liquid correlation energies for local spin density calculations: A critical analysis. *Can. J. Phys.* **58**(8), 1200–1211 (1980).
24. Becke, A. D. Density-functional exchange-energy approximation with correct asymptotic behavior. *Phys. Rev. A* **38**(6), 3098 (1988).
25. Perdew, J. P., Ziesche, P. & Eschrig, H. *Electronic Structure of Solids' 91* (Akademie Verlag, 1991).
26. Perdew, J. P. *et al.* Atoms, molecules, solids, and surfaces: Applications of the generalized gradient approximation for exchange and correlation. *Phys. Rev. B* **46**(11), 6671 (1992).
27. Perdew, J. P. *et al.* Erratum: Atoms, molecules, solids, and surfaces: Applications of the generalized gradient approximation for exchange and correlation. *Phys. Rev. B* **48**(7), 4978 (1993).
28. Perdew, J. P., Burke, K. & Wang, Y. Generalized gradient approximation for the exchange-correlation hole of a many-electron system. *Phys. Rev. B* **54**(23), 16533 (1996).
29. Burke, K., Perdew, J. P. & Wang, Y. Derivation of a generalized gradient approximation: The PW91 density functional. In *Electronic Density Functional Theory* 81–111 (Springer, 1998).
30. Beck, A. D. Density-functional thermochemistry. III. The role of exact exchange. *J. Chem. Phys.* **98**(7), 5648–5646 (1993).
31. Lee, C., Yang, W. & Parr, R. G. Development of the Colle-Salvetti correlation-energy formula into a functional of the electron density. *Phys. Rev. B* **37**(2), 785 (1988).
32. Xu, X. & Goddard, W. A. The X3LYP extended density functional for accurate descriptions of nonbond interactions, spin states, and thermochemical properties. *Proc. Natl. Acad. Sci. USA* **101**(9), 2673–2677 (2004).
33. Becke, A. D. A new mixing of Hartree-Fock and local density-functional theories. *J. Chem. Phys.* **98**(2), 1372–1377 (1993).
34. Yanai, T., Tew, D. P. & Handy, N. C. A new hybrid exchange–correlation functional using the Coulomb-attenuating method (CAM-B3LYP). *Chem. Phys. Lett.* **393**(1–3), 51–57 (2004).
35. Grimme, S. Semiempirical hybrid density functional with perturbative second-order correlation. *J. Chem. Phys.* **124**(3), 034108 (2006).
36. Cížek, J. Advances in chemical physics. *Wiley Intersci.* **14**, 35 (1969).
37. Purvis, G. D. III. & Bartlett, R. J. A full coupled-cluster singles and doubles model: The inclusion of disconnected triples. *J. Chem. Phys.* **76**(4), 1910–1918 (1982).
38. Scuseria, G. E., Janssen, C. L. & Schaefer Iii, H. F. An efficient reformulation of the closed-shell coupled cluster single and double excitation (CCSD) equations. *J. Chem. Phys.* **89**(12), 7382–7387 (1988).
39. Scuseria, G. E. & Schaefer, H. F. III. Is coupled cluster singles and doubles (CCSD) more computationally intensive than quadratic configuration interaction (QCISD)?. *J. Chem. Phys.* **90**(7), 3700–3703 (1989).
40. Frisch, M. *et al. Gaussian 09, Revision d. 01* 201 (Gaussian Inc, 2009).
41. Aidas, K. *et al.* The D alton quantum chemistry program system. *Wiley Interdiscip. Rev.* **4**(3), 269–284 (2014).
42. Hettema, H., Jensen, H. J. R. A., Jorgensen, P. & Olsen, J. Quadratic response functions for a multiconfigurational self-consistent field wave function. *J. Chem. Phys.* **97**(2), 1174–1190 (1992).

43. Luo, Y., Vahtras, O., Ågren, H. & Jørgensen, P. Multiconfigurational quadratic response theory calculations of two-photon electronic transition probabilities of H2O. *Chem. Phys. Lett.* **204**(5–6), 587–594 (1993).
44. Sałek, P. *et al.* Calculations of two-photon absorption cross sections by means of density-functional theory. *Chem. Phys. Lett.* **374**(5–6), 446–452 (2003).
45. Barker, A. D. *et al.* High Performance computing facility operational assessment 2015 Oak Ridge leadership computing facility. *ORNL* 110 (2016).
46. Matxain, J. M., Fowler, J. E. & Ugalde, J. M. Small clusters of II-VI materials: Zn i S i, I = 1–9. *Phys. Rev. A* **61**(5), 053201 (2000).
47. Beljonne, D. *et al.* Two-photon absorption and third-harmonic generation of di-alkyl-amino-nitro-stilbene (DANS): A joint experimental and theoretical study. *J. Chem. Phys.* **103**(18), 7834–7843 (1995).

Acknowledgements

This work is financially supported by the National Natural Science Foundation of China (Grant No. 11974091), and the National Natural Science Foundation of China (Grant No. 51973046).

Author contributions

G.Z. and W.L. designed the study. D.Y. and Y.H. prepared Figs. 1–5. D.Y. and Y.H. wrote and revised the manuscript. G.Z. and Y.J. polished the language. All authors reviewed and approved the final version.

Competing interests

The authors declare no competing interests.

Additional information

Supplementary Information The online version contains supplementary material available at https://doi.org/10.1038/s41598-021-04203-w.

Correspondence and requests for materials should be addressed to G.Z., W.L. or Y.J.

Reprints and permissions information is available at www.nature.com/reprints.

Publisher's note Springer Nature remains neutral with regard to jurisdictional claims in published maps and institutional affiliations.